Electronic Supplementary Material (ESI) for Soft Matter.
This journal is © The Royal Society of Chemistry 2020

[*Electronic Supplementary Information (ESI)*]

Photoinduced Mass Transfer of Azo Polymers from Micrometer to Submillimeter Studied by Real-time Single Particle Strategy

Hao Huang, Chen Zhang, Jiaxing Lan, Zenan Wang and Xiaogong Wang*

Department of Chemical Engineering, Laboratory of Advanced Materials (MOE), Tsinghua University, Beijing 100084, People's Republic of China.

* Corresponding author. Email: wxg-dce@mail.tsinghua.edu.cn

1. Synthesis and characterization

1.1 Precursor polymer (PEMA)

The monomer 2-(ethyl(phenyl)amino)ethyl methacrylate (EMA) was synthesized following our previous report.[S1] CuCl (99%, Sigma-Aldrich) was purified by sequentially washed with excess acetic acid, ethanol and ether for several times, and then dried in the vacuum oven. The precursor polymer PEMA was synthesized by the atom transfer radical polymerization of EMA as follows. EMA (8 g, 34.3 mmol), *p*-toluenesulfonyl chloride (87.3 mg, 0.458 mmol), HMTETA (249 μL, 0.915 mmol) and anisole (13 mL) were added into a 50 mL Schlenk flask. After degassed and back-filled with argon for three times, the solution was frozen in the liquid nitrogen. Then, CuCl (90.6 mg, 0.915 mmol) was quickly added into the flask and the mixture was degassed again through three freeze-pump-thaw cycles. The polymerization was carried out at 50 °C in the oil bath for 10 h and then terminated by cooling with the liquid nitrogen. The obtained mixture was diluted with THF (30 mL) and passed through an alumina column to remove the catalyst. The filtrate was concentrated and added dropwise into petrol ether (500 mL). The precipitated PEMA was purified by repeating the dissolution and precipitation twice in petroleum ether and dried in a vacuum oven at 45 °C for 48 h. Yield: 44%. GPC: M_n = 9500, M_w/M_n = 1.14. ^{1}H NMR (600 MHz, CD_2Cl_2), δ (*ppm*): 7.16 (br, 2H, *m*-Ar H), 6.71 (br, 2H, *o*-Ar H), 6.61 (br, 1H, *p*-Ar H), 4.01 (br, 2H, CH_2), 3.47 (br, 2H, CH_2), 3.34 (br, 2H, CH_2), 1.55-1.95 (m, 2H, -CH_2-C-), 1.11 (br, 3H, CH_3), 0.69-1.02 (m, 3H, CH_3). ^{1}H NMR spectrum and GPC curve of PEMA are shown in Fig. S1 and Fig. S2.

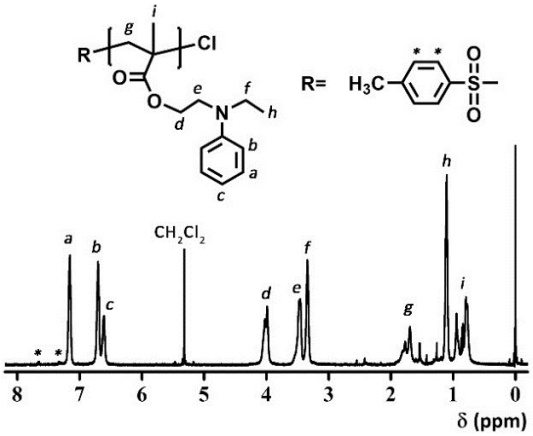

Fig. S1 ^{1}H NMR spectrum of the precursor polymer (PEMA) in CD_2Cl_2. The two small resonances peaked at 7.66 ppm and 7.33 ppm (labelled by asterisks) are attributed to the two sets of aromatic protons in the ATRP initiator (*p*-toluenesulfonyl group).

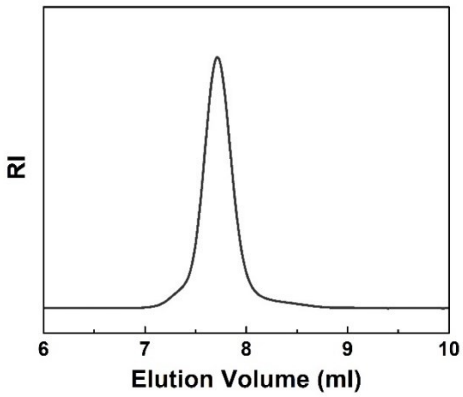

Fig. S2 GPC curve of the precursor polymer (PEMA).

1.2 Characterization of the azo polymers

The synthetic procedure of PEMA-AZs is included in the main text. Their characterization results are shown as follows.

PEMA-AZ-1%: Yield: 85%. GPC: M_n = 9500, M_w/M_n =1.12. ^{1}H NMR (600 MHz, CD_2Cl_2, δ *ppm*): 7.85 (br, 0.05H, *o*-Ar H to N=N in azobenzene moiety), 7.71 (br, 0.03H, *o*-Ar H to CN in azobenzene moiety), 7.15 (br, 1.96H, *m*-Ar H to N– in aniline moiety), 6.45-6.89 (m, 2.93H, including *o*-Ar H, *p*-Ar H to N– in aniline moiety, and *o*-Ar H to N– in azobenzene moiety), 4.01 (br, 2H, CH_2), 3.47 (br, 2H, CH_2), 3.34 (br, 2H, CH_2), 1.45-1.97 (m, 2H, -CH_2-C-), 1.11 (br, 3H, CH_3), 0.65-1.03 (m, 3H, CH_3).

PEMA-AZ-2%: Yield: 85 %. GPC: M_n = 9600, M_w/M_n = 1.14. ^{1}H NMR (600 MHz, CD_2Cl_2, δ *ppm*): 7.85 (br, 0.10H, *o*-Ar H to N=N in azobenzene moiety), 7.71 (br, 0.06H, *o*-Ar H to CN in azobenzene moiety), 7.15 (br, 1.92H, *m*-Ar H to N– in aniline moiety), 6.50-6.89 (m, 2.88H, including *o*-Ar H, *p*-Ar H to N– in aniline moiety, and *o*-Ar H to N– in azobenzene moiety), 4.00 (br, 2H, CH_2), 3.46 (br, 2H, CH_2), 3.34 (br, 2H, CH_2), 1.47-2.00 (m, 2H, -CH_2-C-), 1.10 (br, 3H, CH_3), 0.60-1.02 (m, 3H, CH_3).

PEMA-AZ-5%: Yield: 90%. GPC: M_n = 10100, M_w/M_n = 1.14. ^{1}H NMR (600 MHz, CD_2Cl_2, δ *ppm*): 7.85 (br, 0.22H, *o*-Ar H to N=N in azobenzene moiety), 7.71 (br, 0.12H, *o*-Ar H to CN in azobenzene moiety), 7.15 (br, 1.86H, *m*-Ar H to N– in aniline moiety), 6.45-6.9 (m, 2.79H, including *o*-Ar H, *p*-Ar H to N– in aniline moiety, and *o*-Ar H to N– in azobenzene moiety), 4.01 (br, 2H, CH_2), 3.46 (br, 2H, CH_2), 3.34 (br, 2H, CH_2), 1.45-1.90 (m, 2H, -CH_2-C-), 1.10 (br, 3H, CH_3), 0.65-1.02 (m, 3H, CH_3).

PEMA-AZ-25%: Yield: 92 %. GPC: M_n = 10700, M_w/M_n = 1.17. ^{1}H NMR (600 MHz, CD_2Cl_2, δ *ppm*): 7.82 (br, 1.01H, *o*-Ar H to N=N in azobenzene moiety), 7.69 (br, 0.52H, *o*-Ar H to CN in azobenzene moiety), 7.15 (br, 1.55H, *m*-Ar H to N– in aniline moiety), 6.52-6.89 (m, 2.63H, including *o*-Ar H, *p*-Ar H to N– in aniline moiety, and *o*-Ar H to N– in azobenzene moiety), 3.99 (br, 2H, CH_2), 3.45 (br, 2H, CH_2), 3.32 (br, 2H, CH_2), 1.45-1.96 (m, 2H, -CH_2-C-), 1.09 (br, 3H, CH_3), 0.60-1.01 (m, 3H, CH_3).

PEMA-AZ-100%: Yield: 94 %. GPC: M_n = 11000, M_w/M_n = 1.20. ^{1}H NMR (600 MHz, CD_2Cl_2, δ *ppm*): 7.75 (br, 4H, *o*-Ar H to N=N in azobenzene moiety), 7.63 (br, 2H, *o*-Ar H to CN in azobenzene moiety), 6.45-6.99 (m, 2H, *o*-Ar H to N– in azobenzene moiety), 4.00 (br, 2H, CH_2), 3.50 (br, 2H, CH_2), 3.36 (br, 2H, CH_2), 1.40-2.10 (m, 2H, -CH_2-C-), 1.08 (br, 3H, CH_3), 0.50-0.99 (m, 3H, CH_3).

The *DF* values of PEMA-AZs were determined by their ^{1}H NMR spectra, as shown in Fig. S3. The spectrum of PEMA-AZ-25%, as a typical example, shows six resonance signals in the low field. The resonances a and b, which respectively appear at 7.82 ppm and 7.69 ppm, are attributed to the four protons at *ortho* position to N=N group and the two protons at *ortho* position to -CN group in the azobenzene moiety. In addition, the resonance b overlaps with the resonance signal of the two protons of the ATRP initiator. Considering that the content of azo chromophores in PEMA-AZs could be very low (e.g., *DF* = 1%), which is close to the quantity of initiator, it is necessary to exclude the contribution of the initiator for acquiring a precise *DF* value. The resonance c at 7.15 ppm is attributed to the two protons at *meta* position of aniline group, whose left side also overlaps with the resonance signal of the protons of the ATRP initiator. The set of peak d, e and f, locating at 6.78 ppm, 6.70 ppm and 6.61 ppm, are respectively attributed to the protons at *ortho* position to

amino group in azobenzene moiety, the protons at *ortho* position of aniline moiety and the protons at *para* position of aniline moiety. The above six resonance signals are separated into three groups (peak a+b; peak c; peak d+e+f), and the degree of functionalization (*DF*) is then obtained by using the integral areas of them and following equations,

$$6n_{azo} + 2n_{ini} = I_{a+b} \tag{S1}$$

$$2n_{ani} + 2n_{ini} = I_{c} \tag{S2}$$

$$2n_{azo} + 3n_{ani} = I_{d+e+f} \tag{S3}$$

$$DF = \frac{n_{azo}}{n_{azo} + n_{ani}} = \frac{3I_{a+b} - 3I_{c} + 2I_{d+e+f}}{I_{a+b} - I_{c} + 8I_{d+e+f}} \tag{S4}$$

where the quantity I is the integral area of the resonance signal, n is the molar quantity (a relative value) of each moiety. The subscripts a-f respectively refer to the resonances (a-f) as labelled in Fig. S3. The subscript azo, ani, ini represents the structure unit containing azobenzene, the structure unit containing aniline, and the ATRP initiator (p-toluenesulfonyl group), respectively. The feed ratio and calculated *DF* values of PEMA-AZs are listed in Table S1.

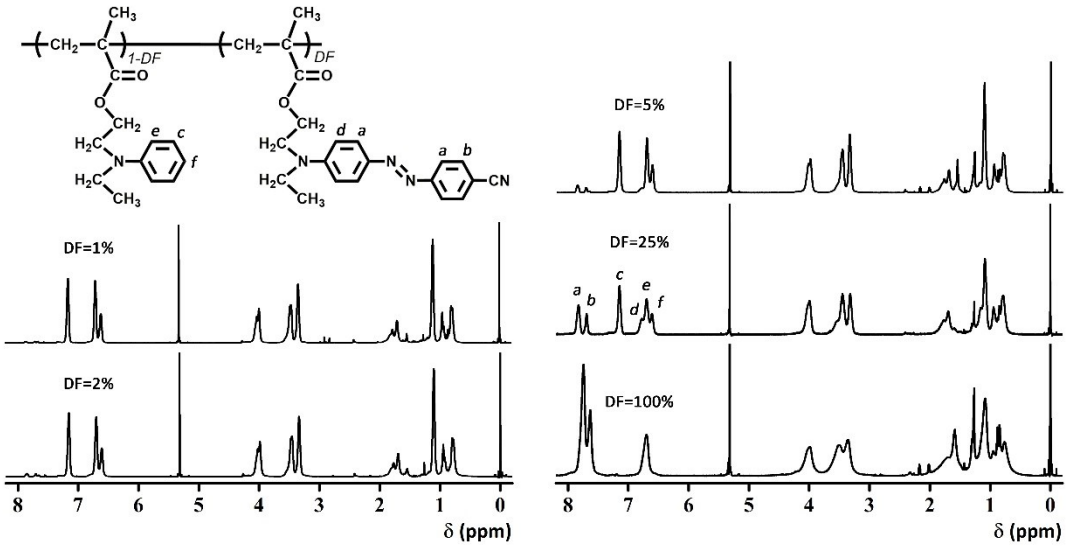

Fig. S3 ^{1}H NMR spectra of the azo polymers (PEMA-AZs) with different *DF*s.

Table S1. *DF* values of the PEMA-AZs with different feed ratios.

Sample name	PEMA-AZ-1%	PEMA-AZ-2%	PEMA-AZ-5%	PEMA-AZ-25%	PEMA-AZ-100%
Feed ratio (%) [a]	1.2	2.4	6	30	120
I_c / I_{a+b}	17.64	10.81	5.16	1.01	0.01
I_{d+e+f} / I_{a+b}	26.07	16.11	7.72	1.72	0.33
Calculated *DF* (%) [b]	1.16	2.34	5.14	24.8	100.0

[a] The feed ratio is defined as the molar ratio between the 4-aminobenzonitrile and the aniline group in PEMA.
[b] The round figures of the calculated *DF*, 1%, 2%, 5%, 25% and 100%, are used for the identifying the azo polymers.

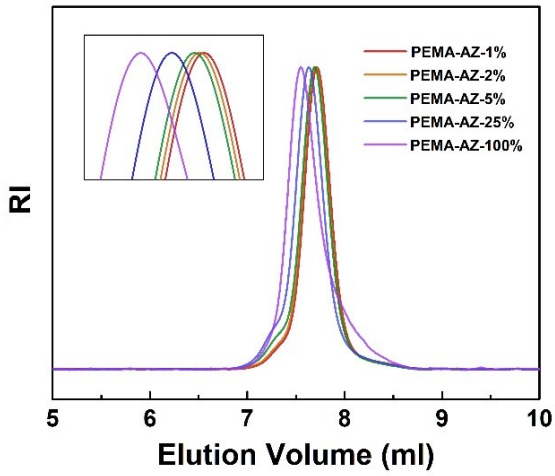

Fig. S4. GPC curves of PEMA-AZs with different *DF*s. The inset is the magnified image of the GPC curves around the elution peak.

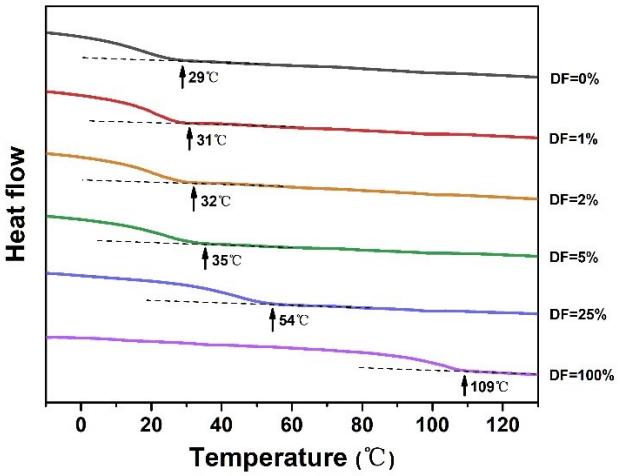

Fig. S5. DSC curves of PEMA and PEMA-AZs with different *DF*s. The glass transition temperature (T_g) is indicated below each curve.

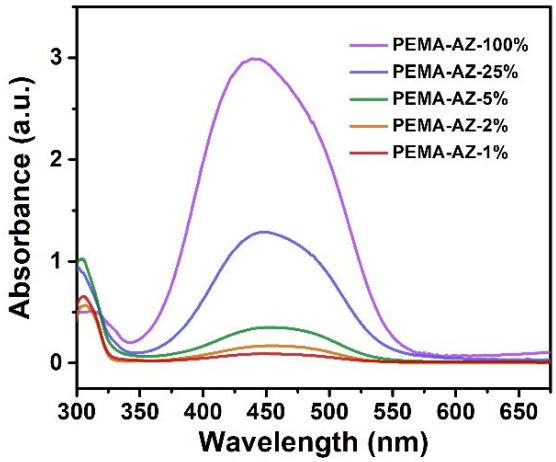

Fig. S6. UV-vis spectra of PEMA-AZs films. The thicknesses of the films were about 500 nm.

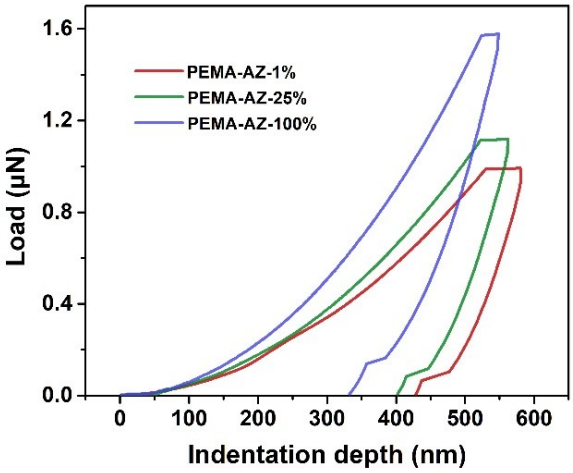

Fig. S7. The nanoindentation curves of PEMA-AZs with different *DF*s, from which their elastic modulus (*E*) and hardness (*H*) can be evaluated. For *DF* of 1%, 25% and 100%, *E* is respectively 4.3 GPa, 4.3 GPa and 4.7 GPa, and *H* is respectively 0.17, 0.2, 0.3 GPa. Therefore, although the *DF* value varies in a range of the two orders of magnitude, their mechanical properties are still within the same order of magnitude.

Table S2. Optical properties of PEMA-AZs at the wavelength of 532 nm.

***DF* (%)**	**1%**	**2%**	**5%**	**25%**	**100%**
Refractive index (*n*)	1.582	1.609	1.635	1.818	2.069
Extinction coefficient (κ)	0.001	0.002	0.012	0.037	0.158
Light penetration depth [a]	195 μm	97 μm	16 μm	5 μm	1 μm

[a] The light penetration depth is defined as the propagation distance of 532 nm light in azo polymer till the intensity attenuates to 1% of the incident intensity, which was calculated following the Beer's Law, $I = I_0\exp(-4\pi\kappa z/\lambda_0)$.[S2]

2. Optical microscopy images of the azo polymer microspheres

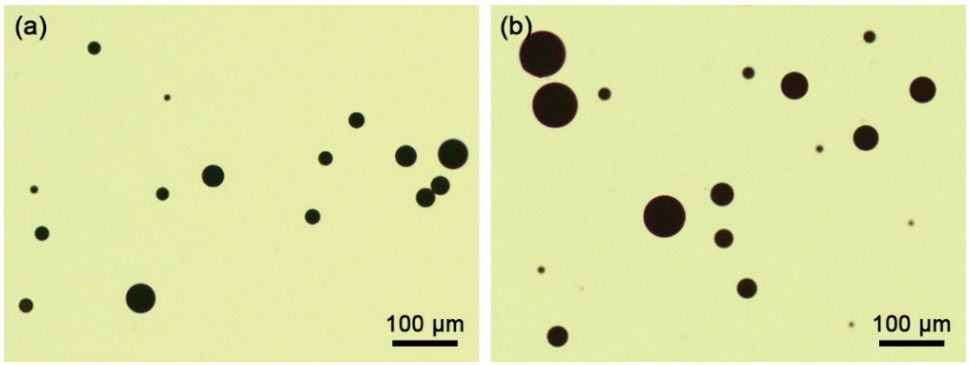

Fig. S8. Typical optical microscope (OM) images of the PEMA-AZ-25% microspheres on the glass substrate. As the microspheres were fabricated by the emulsion-solvent evaporation method, they exhibited a wide range of sizes from several micrometers to hundred micrometers. On the other hand, it showed that the azo polymer microspheres could be dispersedly loaded on the glass substrate as isolated particles by drop-casting and properly drying.

3. Additional results of the photoinduced deformation test

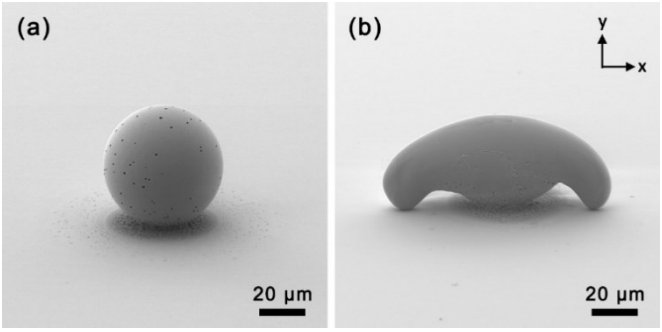

Fig. S9. SEM images of (a) the PEMA-AZ-5% microsphere (D = 53 μm) and (b) the deformed particle after 532 nm laser irradiation for 5 min. The morphology was observed from a same viewing angle as the real-time OM observation in the main text. The coordinate system is indicated in (b).

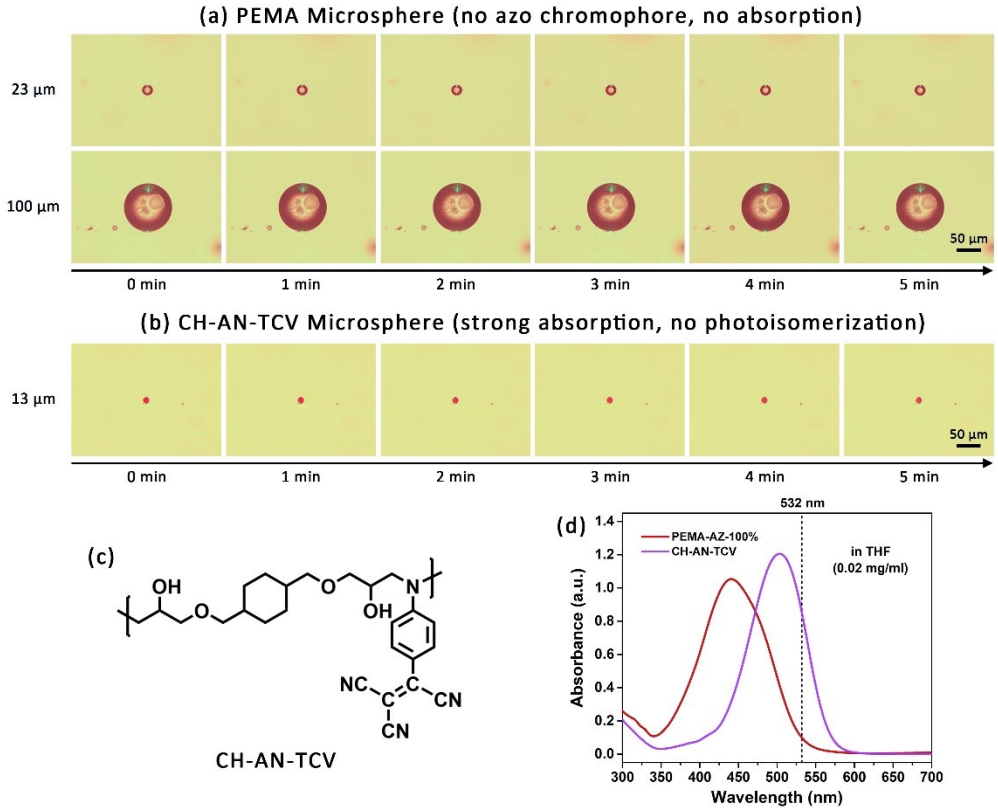

Fig. S10. Real-time OM images of (a) PEMA microspheres (D = 23 μm and 100 μm) and (b) CH-AN-TCV microspheres (D = 13 μm) upon 532 nm laser irradiation with the intensity of 10 W/cm^2. PEMA is the precursor polymer, which contains no azo chromophores and shows no absorption at 532 nm. The polymer CH-AN-TCV contains 4-tricyanovinylaniline groups (Fig. S10(c)), which was synthesized following our previous work.[S3] CH-AN-TCV shows much stronger light absorption than the azo polymer PEMA-AZ-100% at 532 nm (Fig. S10(d)), while it does not possess photoisomerization function of the azo chromophore. As shown in Fig. S10(a, b), no obvious deformation or shape variation can be observed for both the PEMA microspheres and CH-AN-TCV microspheres. It is proved that the unique photoinduced deformation observed for PEMA-AZs microspheres is solely related to the photoresponsive function of the azo chromophores.

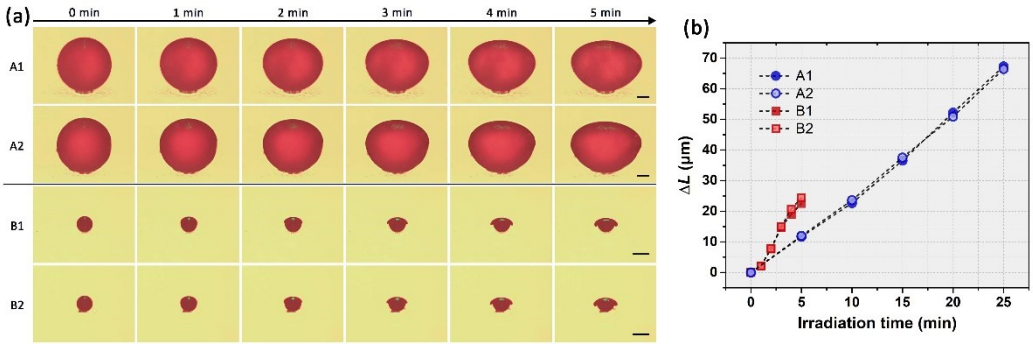

Fig. S11. A repeatability test of photoinduced deformation, (a) OM images of the shape evolutions for two independent experiments in each group, (b) the quantitative results of the elongation degrees of particles obtained from (a). Two groups of azo polymer microspheres were used. For A1 and A2 in the figure, the azo polymer is PEMA-AZ-1% and the diameter is about 220 μm. For B1 and B2 in the figure, the azo polymer is PEMA-AZ-25% and the diameter is about 50 μm. The scale bars in (a) are all 50 μm. As indicated in (a), the photo-fabricated morphologies are almost identical for the two independent experiments in each group, comparing A1 with A2 or B1 with B2, which only show negligible random differences. The quantitative comparison given in (b) further confirms this point.

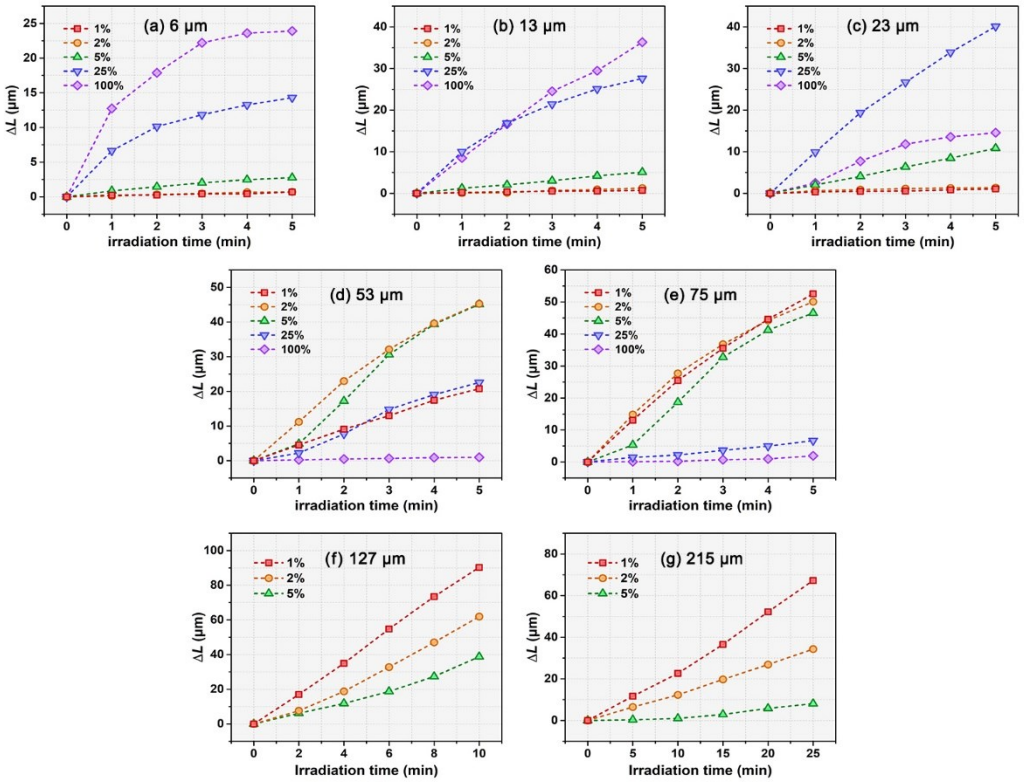

Fig. S12. Variation of elongation degree (ΔL) of the PEMA-AZs microspheres with the light irradiation time. The diameters (D) of the microspheres range from micrometer to submillimeter scale. For $D < 100$ μm, the laser intensity of 10 W/cm^2 was used; for $D = 127$ and 215 μm, the laser intensity was 5 W/cm^2 and 2 W/cm^2, respectively.

4. Optical simulation methods and results

The light propagation, attenuation and optical power distribution in the PEMA-AZs microspheres are simulated by the ray optics method.[S4] The microsphere with diameter of D is irradiated by the 532 nm linearly polarized light. A right-handed Cartesian coordinate system is set up with the x-axis parallel to the electric vibration of incident light and the −y direction parallel to light propagation (Fig. S13). The origin O(0, 0, 0) is fixed at the microsphere center. The complex refractive indices (n+iκ) of PEMA-AZs at the wavelength of 532 nm were measured by ellipsometry (Table S2) and used for the optical simulation. The xOy cross-section of the microsphere corresponds with the projection plane in real-time observation and the maximum cross-section of the photo-deformed particles as well, which is selected as the plane of investigation for optical simulation.

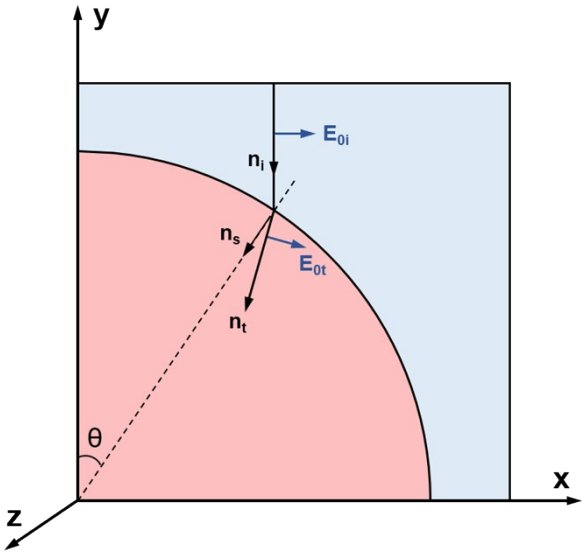

Fig. S13. Illustration of the propagation direction and electric field of the incident and refracted rays.

Firstly, the light refraction on the microsphere surface is analyzed following Snell's law and Fresnel equations. For the point of incidence (Rsin(θ), Rcos(θ), 0), where R is the radius of a microsphere, the surface normal and the propagation of incident light are given by the following unit vectors, respectively,

$$\mathbf{n}_s = (-\sin(\theta_i), -\cos(\theta_i), 0) \tag{S5}$$

$$\mathbf{n}_i = (0, -1, 0) \tag{S6}$$

where the subscripts s and i denote the microsphere surface and the incident light, respectively. The angle of incidence θ_i is equal to the zenith angle θ for a spherical surface. According to the Snell's Law, the angle of refraction θ_t is,

$$\theta_t = \arcsin(\sin(\theta_i)/n) \tag{S7}$$

where the subscript t denotes the refracted light. In addition, the propagation direction of refracted light is given by vectorial form of Snell's Law,

$$\mathbf{n}_t = \mu \mathbf{n}_i + \gamma \mathbf{n}_s \tag{S8}$$

where,

$$\mu = \frac{1}{n} \tag{S9}$$

$$\gamma = -\mu \cos(\theta_i) + \cos(\theta_t) \tag{S10}$$

By combining Equation (S5-S10), we have,

$$\mathbf{n}_t = -(\sin(\theta_i - \theta_t), \cos(\theta_i - \theta_t), 0) \tag{S11}$$

As the electric field of incident light ($\mathbf{E}_{0i}$) is parallel to the plane of incidence (xOy plane) without components perpendicular to that (see Fig. S13), the amplitude transmission coefficient can be directly calculated following the Fresnel equation,

$$t = t_P = \left(\frac{E_{0t}}{E_{0i}} \right)_P = \frac{E_{0t}}{E_{0i}} = \frac{2\cos(\theta_i)}{n\cos(\theta_i) + \cos(\theta_t)} \tag{S12}$$

where the subscript || denotes the component parallel to the plane of incidence, E_{0i} and E_{0t} are the electric field amplitudes for the incident light and refracted light at the interface (where the propagation distance of refracted light is 0), respectively.

The intensity and power of the refracted light at the interface is respectively expressed as,

$$I_{0t} = \frac{n}{2c\mu_0} E_{0t}^2 = n I_{0i} t^2 \tag{S13}$$

$$P_{0t} = \frac{\cos(\theta_t)}{\cos(\theta_i)} n P_{0i} t^2 \tag{S14}$$

where c and μ_0 are the light speed and permeability in vacuum, I_{0i} and P_{0i} are the intensity and power of each incident light ray.

As light is refracted on the curved surface of microsphere, the curvatures of wavefront between the refracted light and the incident light are different (Fig. S14). Generally, the curvatures of wavefront are characterized by its two principle radii of curvatures (ρ_1, ρ_2) along the principle curvature directions ($\mathbf{u}_1$,$\mathbf{u}_2$). In fact, ($\mathbf{u}_1$,$\mathbf{u}_2$,$\mathbf{n}$) constituents a set of base vectors of a right-handed Cartesian coordinate system, where $\mathbf{n}$ is the unit vector of propagation direction. The principle radii of curvatures of refracted wavefronts in the microsphere can be calculated as follows.

The normal direction of the plane of incidence is,

$$\mathbf{u}_0 = \mathbf{n}_i \times \mathbf{n}_s \tag{S15}$$

Three other unit vectors are defined as,

$$\mathbf{u}_i = \mathbf{n}_i \times \mathbf{u}_0 \tag{S16}$$

$$\mathbf{u}_s = \mathbf{n}_s \times \mathbf{u}_0 \tag{S17}$$

$$\mathbf{u}_t = \mathbf{n}_t \times \mathbf{u}_0 \tag{S18}$$

which is respectively tangent to the incident wavefront, microsphere surface and the refracted wavefront. As the size of microsphere is much smaller than that of the laser spot and they are concentric with each other as well, the incident Gaussian beam can be regarded as a plane wave. In other words, the curvature tensor of incident wavefront is a zero matrix,

$$K_{1,\mathrm{i}} = K_{2,\mathrm{i}} = K_{12,\mathrm{i}} = 0 \tag{S19}$$

where $K_{1,\mathrm{i}}$ and $K_{2,\mathrm{i}}$ are the diagonal elements of wavefront curvature tensor, and $K_{12,\mathrm{i}}$ is the off-diagonal element of it. Consequently, $\mathbf{u}_0$ and $\mathbf{u}_\mathrm{i}$ can be chosen as the two principle curvature directions, along which the principle curvatures are both zero.

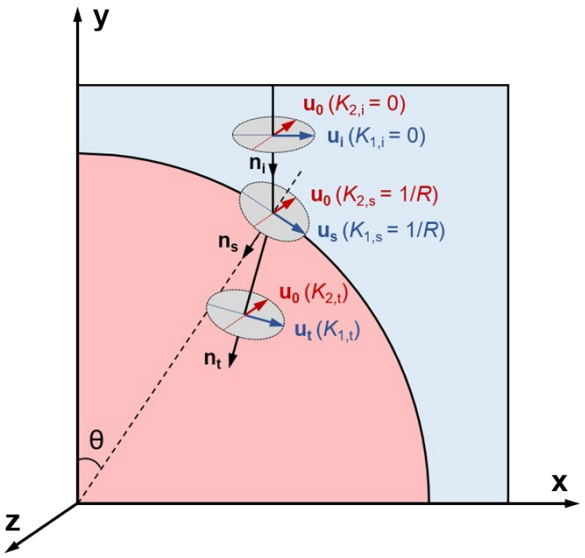

Fig. S14. Illustration of the principle curvatures and principle curvature directions of the incident wavefront, microsphere surface, and the refracted wavefront.

The curvature tensor of the microsphere surface is,

$$K_{1,\mathrm{s}} = K_{2,\mathrm{s}} = 1/R \tag{S20}$$

$$K_{12,\mathrm{s}} = 0 \tag{S21}$$

Similarly, $\mathbf{u}_0$ and $\mathbf{u}_\mathrm{s}$ can be regarded as the two principle curvature directions of the microsphere surface, along which the principle curvatures are both $1/R$. Now, the principle curvatures of the incident wavefront and the surface have a shared axis ($\mathbf{u}_0$), and their un-shared axes ($\mathbf{u}_\mathrm{i}$ and $\mathbf{u}_\mathrm{s}$) show an intersection angel of θ_i. In this situation, the curvature tensor of refracted wavefront can be calculated by the following expressions,[S4]

$$K_{1,\mathrm{t}} = \mu K_{1,\mathrm{i}} + \gamma K_{1,\mathrm{s}} \tag{S22}$$

$$K_{2,\mathrm{t}} = \frac{\mu \cos^2(\theta_\mathrm{i}) K_{2,\mathrm{i}}}{\cos^2(\theta_\mathrm{t})} + \frac{\gamma K_{2,\mathrm{s}}}{\cos^2(\theta_\mathrm{t})} \tag{S23}$$

$$K_{12,\mathrm{t}} = \frac{\mu \cos(\theta_\mathrm{i}) K_{12,\mathrm{i}}}{\cos(\theta_\mathrm{t})} + \frac{\gamma K_{12,\mathrm{s}}}{\cos(\theta_\mathrm{t})} = 0 \tag{S24}$$

where $K_{1,t}$ and $K_{2,t}$ are the wavefront curvature along $\mathbf{u}_0$ and $\mathbf{u}_t$, respectively. Noting that the off-diagonal element $K_{12,t}$ is zero, $K_{1,t}$ and $K_{2,t}$ are the eigenvalues of the curvature tensor. In other words, the two principle curvatures of refracted light are exactly $K_{1,t}$ and $K_{2,t}$, with the principle curvature directions along $\mathbf{u}_0$ and $\mathbf{u}_t$, respectively. Hence, the principle radii of curvature of refracted light (at the interface) are,

$$\rho_{1,t} = 1/K_{1,t} = \frac{nR}{n\cos\theta_t - \cos\theta_i} \tag{S25}$$

$$\rho_{2,t} = 1/K_{2,t} = \frac{nR\cos^2\theta_t}{n\cos\theta_t - \cos\theta_i} \tag{S26}$$

For the refracted wavefront in the microsphere domain, its principle radii of curvature vary with the propagation distance (s) at a constant rate,

$$\frac{d\rho}{ds} = -1 \tag{S27}$$

which can be also expressed by,

$$\rho_1 = \rho_{1,t} - s \tag{S28}$$

$$\rho_2 = \rho_{2,t} - s \tag{S29}$$

According to Equation (S25 and S26), the radii of curvature at the interface ($\rho_{1,t}$, $\rho_{2,t}$) are positive, which represents a converging wavefront and contributes to increase the light intensity with its propagation. In addition, as the imaginary part of complex refractive index of PEMA-AZs is none-zero, there also occurs light attenuation with its propagation, which follows the differential form of Lambert-Beer's law,

$$dI_{absorb} = -\frac{4\pi\kappa}{\lambda_0} I ds \tag{S30}$$

where dI_{absorb} refers to the variation of light intensity due to the optical absorption when the light propagates for a small distance of ds, I is the initial light intensity, and λ_0 is the vacuum wavelength.

Therefore, for the calculation of light intensity in PEMA-AZ microsphere, the effect of principle radii of curvature and light attenuation should be both considered,

$$IS + dI_{absorb}S = (I + dI)(S + dS) \tag{S31}$$

where S equals to $\rho_1\rho_2$, which represents the area of the refracted wavefront. By combining Equation (S28-S31), we have

$$\frac{dI}{I} = -\left(\frac{1}{s - \rho_{1,t}} + \frac{1}{s - \rho_{2,t}} + \frac{4\pi\kappa}{\lambda_0}\right) ds \tag{S32}$$

Then, the analytical expression of the intensity of refracted light can be obtained by solving the above differential equation, which is

$$I = I_{0t} \frac{\rho_{1,t}\rho_{2,t}}{\left|s - \rho_{1,t}\right|\left|s - \rho_{2,t}\right|} \exp\left(-\frac{4\pi\kappa}{\lambda_0} s\right) \tag{S33}$$

Consequently, the light attenuation of the refracted rays is affected by parameters including the microsphere diameter (D), degree of functionalization (DF) as well as the incident angle (θ_i). Using this equation, we simulated the light propagation and attenuation behavior in PEMA-AZ-5% microspheres with three typical diameters (D = 23, 53 and 75 μm), whose results are visualized in Fig. 7 in the main text.

The light penetration depth ($s_{1\%}$) in PEMA-AZs microspheres is defined as the propagation depth of the refracted light with $\theta = \theta_i = \theta_t = 0$ (normal to the top surface of microsphere) till its intensity attenuates to 1% of the incident intensity, which is obtained by solving the following equation,

$$1\% = \frac{nt^2\rho_0^2}{(s_{1\%} - \rho_0)^2}\exp(-\frac{4\pi\kappa}{\lambda_0}s_{1\%}) \tag{S34}$$

where

$$\rho_0 = \frac{nR}{n-1} \tag{S35}$$

The light penetrated ratio (R_p) of PEMA-AZs microspheres is then evaluated by the ratio between light penetration depth in the microspheres ($s_{1\%}$) and the microsphere diameter (D).

On the other hand, for acquiring the distribution of optical power in the microsphere, it is more convenient to directly calculate the power of each refracted light rays other than the light intensities, which follows

$$P = P_{0t}\exp(-\frac{4\pi\kappa}{\lambda_0}s) \tag{S36}$$

whose difference form is

$$-\Delta P = \frac{4\pi\kappa}{\lambda_0}P_{0t}\exp(-\frac{4\pi\kappa}{\lambda_0}s)\Delta s \tag{S37}$$

where $-\Delta P$ refers to the power loss when the ray passes through a new distance of Δs after being propagated for s. Compared to the variation of light intensity (Equation S33), the variation of ray power is not affected by the principle radii of curvature. The effect of the wavefront convergence in the microsphere is included by gridding the microsphere domain and summing $-\Delta P$ within each mesh. The absorbed power density (q_a) of each mesh is calculated by

$$q_a = \frac{\sum_{mesh}(-\Delta P)}{V_{mesh}} \tag{S38}$$

The q_a distribution in the xOy cross-section of PEMA-AZs microspheres for several typical cases are drawn in Fig. 8 in the main text. The simulation results for all the cases can be seen in Fig. S15 and Fig. S16.

Finally, the optical absorption efficiency (E_a) is calculated, which is defined as the ratio between the total optical power absorbed by the microsphere and that of the incident rays projected to it,

$$E_a = \frac{Q_{absorb}}{Q_{input}} = \frac{\sum(q_a \times V_{mesh})}{\sum P_i} = \frac{\sum(-\Delta P)}{\sum P_i} \tag{S39}$$

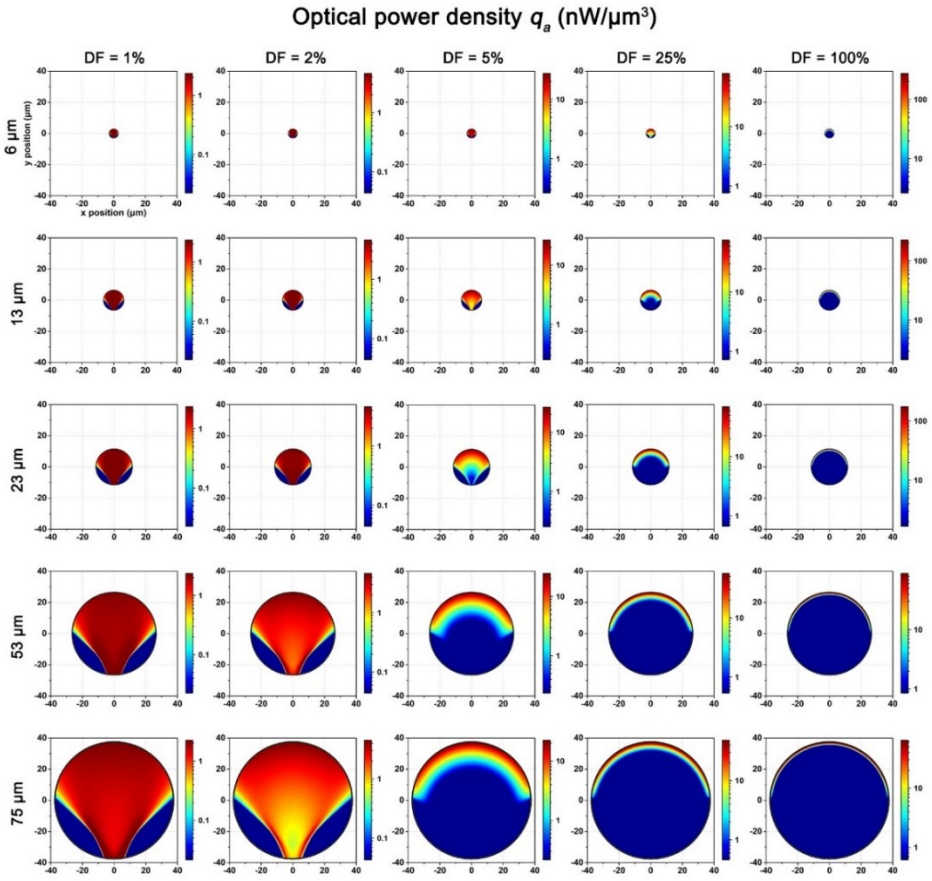

Fig. S15. Distribution of the optical power density (q_a) received in PEMA-AZs microspheres upon 532 nm laser irradiation. The 5×5 panels represent the cases with diameters from 6 μm to 75 μm and with *DF* from 1% to 100%, respectively. The results are selectively presented in the xOy cross-section of microsphere, which corresponds with the projection plane in real-time observation. The colormap uses logarithmic scale.

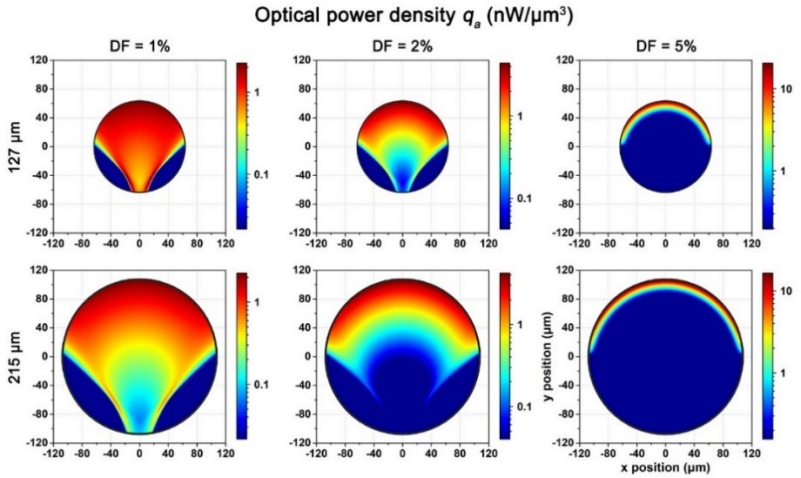

Fig. S16. Distribution of the optical power density (q_a) received in PEMA-AZs microspheres upon 532 nm laser irradiation. The 2×3 panels represent the cases with diameter from 127 μm to 215 μm and with *DF* from 1% to 5%, respectively. The calculated results are selectively presented in the xOy cross-section of microsphere, which corresponds with the projection plane in real-time observation. The colormap uses logarithmic scale.

5. Thermal effect calculation methods and results

The photothermal effect of PEMA-AZs microspheres upon laser irradiation is evaluated as follows. The absorbed optical power density (q_a) in the microsphere acts as a heat source of each domain and raises the temperature. Due to the relatively small size scale of the microspheres (from micrometer to submillimeter), the heat conduction within it is assumed to be very efficient. Hence, the microsphere is regarded as a single heat source with a uniform temperature distribution. Noteworthy, the glass substrate shows no temperature increase as it is transparent at the wavelength of 532 nm. The total heat power (Q_{ray}, the integral of the absorbed optical power density in the microsphere) can be calculated from the absorption efficiency (E_a) obtained by the optical simulation results, which follows,

$$Q_{ray} = \int_{\Omega} q_a \, dV = \pi R^2 I E_a \tag{S40}$$

where R is the radius of microsphere and I is the intensity of the incident light (unit: $W \cdot m^{-2}$). On the other hand, the natural convection on the microsphere surface dominates the process to dissipate the heat and cool the microsphere, and the heat conduction to the glass substrate is very weak due to the small contact area with the particle. The total power of convective heat transfer is expressed by,

$$Q_c = hS(T_{azo} - T_{air}) = 4\pi R^2 h(T_{azo} - T_{air}) \tag{S41}$$

where h is the heat transfer coefficient of the microsphere surface (unit: $W \cdot m^{-2} \cdot K^{-1}$), T_{azo} is the temperature of the microsphere (unit: K), and T_{air} is the temperature of the ambient air (293.15 K). The natural convection heat transfer coefficient for the spherical geometry is obtained from reference,[S5]

$$h = \frac{k}{D}\left\{2 + \frac{0.589 Ra_D^{0.25}}{\left[1 + \left(\frac{0.469}{\mu C_p k}\right)^{9/16}\right]^{4/9}}\right\}^2 \tag{S42}$$

$$Ra_D = \frac{g\alpha_p \rho^2 C_p (T_{azo} - T_{air}) D^3}{k\mu} \tag{S43}$$

where Ra_D is the Rayleigh number; k is the thermal conductivity of air (unit: $W \cdot m^{-1} \cdot K^{-1}$); D is the diameter of microsphere (unit: m); μ is the dynamic viscosity of air (unit: Pa·s); C_p is the heat capacity at constant pressure of air (unit: $J \cdot kg^{-1} \cdot K^{-1}$); g is the acceleration of gravity (unit: $m \cdot s^{-2}$); ρ is the density of air (unit: $kg \cdot m^{-3}$); α_p is the coefficient of thermal expansion of air (unit: K^{-1}).

The physical properties of air are obtained using their values at the temperature of $(T_{azo}+T_{air})/2$. The validity of the equation is verified by evaluating the following criteria,

$$Ra_D \le 10^{11} \text{ and } Pr = \mu C_p k \ge 0.7 \tag{S44}$$

The temperature of microsphere at heat balance is evaluated by combining the ray heating effect (Equation S40) and the natural convection heat transfer (Equation S41), following

$$T_{azo} = \frac{IE_a}{4h} + T_{air} \tag{S45}$$

As h is also the function of temperature, the exact solution of T_{azo} is obtained by solving Equation (S42), (S43) and (S45) by the least square method. The results are listed in Table S3 and S4. In addition, the heat transfer coefficient, when $(T_{azo}+T_{air})/2$ is 30 °C, is also given to illustrate the relationship between convective heat transfer performance of microspheres with their diameters, as shown in Table S5.

Table S3. Calculated temperature (unit: °C) of PEMA-AZs microspheres (D < 100 μm) upon laser irradiation with intensity of 10 W·cm^{-2}.

D **(μm)**	***DF*** **(%)**				
	1%	**2%**	**5%**	**25%**	**100%**
6	20.2	20.3	21.1	21.4	21.4
13	20.8	21.3	22.9	23.0	22.9
23	22.1	23.4	25.3	25.2	25.1
53	28.2	30.7	31.8	31.6	31.3
75	33.2	35.7	36.2	36.0	35.6

Table S4. Calculated temperature (unit: °C) of PEMA-AZ-1% microspheres (D > 100 μm) upon laser irradiation with different intensities.

D **(μm)**	***I*** **(W·m^{-2})**		
	10	**5**	**2**
127	44.5	32.6	25.2
215	60.2	41.0	28.8

Table S5. Heat transfer coefficient of the microspheres with different diameters evaluated at the temperature of 30 ℃.

D **/ μm**	**6**	**13**	**23**	**53**	**75**	**121**	**215**
h / W·m^{-2}·K^{-1}	17178	7988	4556	2022	1450	882	544

6. Shape evolution results upon irradiation with different light intensities

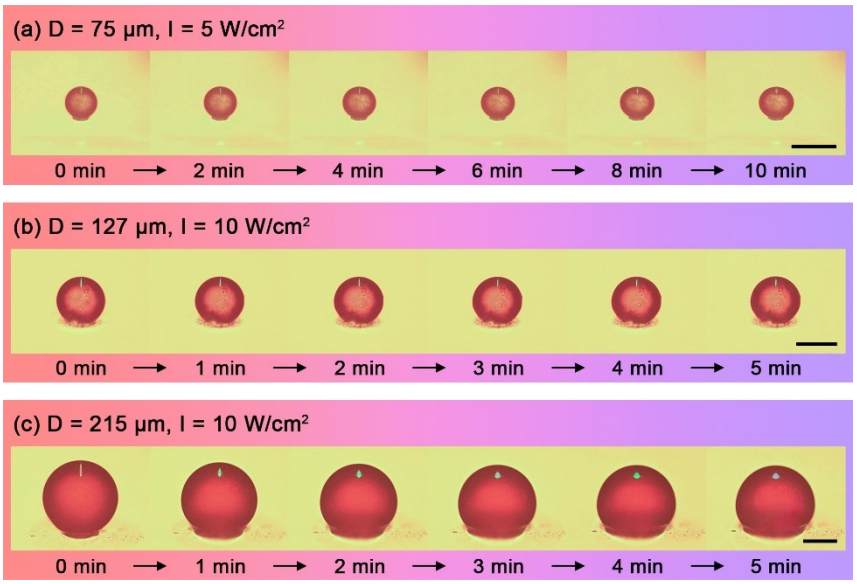

Fig. S17. Real-time OM images of the PEMA-AZ-1% microspheres with the diameters of (a) 75 μm, (b) 127 μm and (c) 215 μm upon 532 nm laser irradiation. The scale bars are 100 μm. As observed, the light intensities used in these three cases were all unable to induce the significant mass transfer for the microspheres with the corresponding diameters. Especially, for the case shown in (c), as the temperature of microsphere rises to about 60 ℃ upon laser irradiation (see Table S4), much higher than the T_g of PEMA-AZ-1%, the particle is gradually collapsed to the glass substrate driven by the gravity and surface tension.

References

[S1] D. R. Wang, G. Ye and X. G. Wang, *Macromol. Rapid Comm.*, 2007, **28**, 2237-2243.

[S2] M. Fox, *Optical Properties of Solids*, Oxford University Press, New York, 2001.

[S3] Y. Q. Zhou, B. Y. Liu and X. G. Wang, *Polymer*, 2016, **97**, 1-10.

[S4] O. Stavroudis, *The Optics of Rays, Wavefronts, and Caustics*, Academic Press, New York, 1972.

[S5] F. P. Incropera, D. P. DeWitt, T. L. Bergman and A. S. Lavine, *Fundamentals of Heat and Mass Transfer*, *6th ed.*, John Wiley & Sons, New York, 2006.